

Constraining rotating black holes in Horndeski theory with *EHT* observations of M87*

MISBA AFRIN ¹ AND SUSHANT G. GHOSH ^{1,2}

¹*Centre for Theoretical Physics, Jamia Millia Islamia, New Delhi 110025, India*

²*Astrophysics and Cosmology Research Unit, School of Mathematics, Statistics and Computer Science, University of KwaZulu-Natal, Private Bag 54001, Durban 4000, South Africa*

ABSTRACT

To explicate the astrophysical nature of the M87* black hole, we resort to rotating hairy black holes in the framework of Horndeski gravity, which, besides mass M and spin a , have an additional hair parameter h . We investigate various spacetime properties of these black holes viz., the horizon structure and shadow geometry to deduce that an increase in the hair h from the Kerr limit ($h \rightarrow 0$) reduces the horizon radii but increase the shadow size alongside inducing a more significant distortion in the shadow shape. Further, we find that the nature of the dependence of the shadow structure on the a and h may cause degeneracy of the various astronomical observables like the shadow area A and oblateness D , in the black hole parameters. Thus we use a simple contour intersection method to infer that the astronomical observables can uniquely determine the spin and hair parameter. Using the Event Horizon Telescope (*EHT*) observations, we find that within 1σ uncertainty of the astronomical measurements, the inferred circularity deviation $\Delta C \leq 0.1$ for the M87* black hole is satisfied for the entire parameter space of the rotating Horndeski black holes. However, the shadow angular diameter $\theta_d = 42 \pm 3 \mu\text{as}$ places tight upper bounds on both a and h , at both 90° and 17° observation angles. Within this consistent parameter region (a - h) where the rotating Horndeski black holes are viable candidates for the M87*, we carry out a systematic bias analysis and find that the reduced χ^2 between the shadow observables A and D of the rotating black holes in the Horndeski theory and the Kerr black hole is > 1 for a substantial parameter region. Thus our present study elucidates the distinguishability of the Horndeski theory from GR and motivates the test of the GR against the alternative theory of Horndeski gravity using the astrophysical observations viz., using the *EHT* at its current resolution.

Keywords: Astrophysical black holes (98); Galactic center (565); Black hole physics (159); Gravitation (661); Gravitational lensing (670)

1. INTRODUCTION

According to General Relativity (GR) and its no-hair theorem (Carter 1971), black holes are only characterized by three gauge charges (or “hairs”), i.e. mass, spin and electric charge (Israel 1967; Hawking 1972). The charge of astrophysical black holes is expected to be negligible, viz., the charge of the galactic centre black hole Sgr A*, was recently estimated to be $\lesssim 3 \times 10^8 C$ (i.e. $4 \times 10^{-19}M$ in terms of the black hole mass) (Zajaček et al. 2018). Since the electric charge is expected to be tiny or spontaneously lost in realistic environments (Gibbons 1975), astrophysical BHs are de-

scribed by Kerr geometry in GR. Undoubtedly, has GR served as a very well tested standard model of gravity but is not devoid of inconsistencies both in the ultra-violet (UV) (Goroff & Sagnotti 1986) and infrared (IR) (Weinberg 1989) energy scales, whereby, GR needs extensions (Cisterna et al. 2016). Nonetheless, modified theories of gravity have been explored actively mainly due to several quantum field theoretical and cosmological reasons: the pathological occurrence of ghost degrees of freedom due to renormalization of higher-order GR theories (Stelle 1977), the occurrence of singularity (Psaltis 2008), the anomalous acceleration of Pioneer (Anderson et al. 2002), the experimental evidences suggesting the need for more than 95% of our Universe to be made from dark matter (Zwicky 1933) and dark energy (Sako et al. 2018; Sievers et al. 2013; Dawson et al.

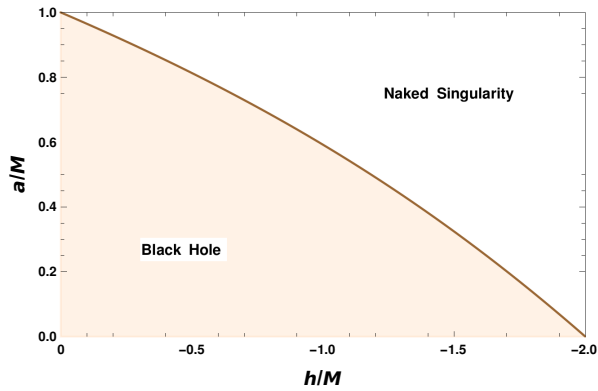


Figure 1. The parameter space ($a - h$) of the rotating Horndeski black hole. The solid line separating black holes from naked singularities corresponds to extremal black holes.

2013) and a need to incorporate modifications for theoretical consistency in the UV region (Horava 2009).

The above as well as several other recent developments in astrophysics and cosmology beyond GR, incur interest in various scalar-tensor theories of gravity. Studies on the late time acceleration and inflationary phase of the Universe have called for the coupling of GR to scalar fields (Brito & Santos 2020). These efforts led to the development of the well-known generalized Galileons which can be mapped to the most general scalar-tensor theory in four dimensions (for e.g. see (Damour & Esposito-Farese 1992; Horbatsch et al. 2015) for tensor-multiscalar theories, and (Padilla & Sivanesan 2013; Charmousis et al. 2014) for multiscalar versions of Horndeski gravity) with second-order field equations (of a scalar field ϕ) and second-order energy-momentum tensor (Nicolis et al. 2009), first proposed by Gregory Horndeski in 1974 (Horndeski 1974) and termed the Horndeski theory. Besides the cosmological reasons, several exciting investigations in astrophysics lead *a fortiori* to various black hole solutions in the Horndeski theory: Hawking-Page phase transition in context of asymptotically locally anti de Sitter and flat black holes (Anabalon et al. 2014), constraints from perihelion precession and gravitational bending angle of light in spherically symmetric black holes in Horndeski framework (see, Bhattacharya & Chakraborty 2017, and the references therein) and upper bound on Galelian charge of an exact black hole solution in Horndeski gravity using the the Gravity Probe B results (Mukherjee & Chakraborty 2018) are few recent investigations. Furthermore, solutions of astrophysical compact objects have also been considered viz., the construction and analysis of boson stars in in the biscalar extension of Horndeski gravity (Brihaye et al. 2016) and slowly rotating neutron stars

in the nonminimal derivative coupling sector of Horndeski gravity (Cisterna et al. 2016).

To test Einstein's GR and to ultimately find out the correct (effective low energy and high energy) description of gravity, we need to know the theoretical predictions of other theories as well. Besides academic interests, this motivation is ever increasing after the first detection of gravitational waves (Abbott et al. 2016) and the first image of the supermassive black hole M87* by the Event Horizon Telescope collaboration (EHT) (Akiyama et al. 2019a,b,c). As an interferometer using the Very Long Baseline Interferometry (VLBI) technique, the EHT has recently measured the Fourier components of the brightness distribution of the supermassive black hole (SMBH) M87* emission region and the features of the underlying image have then been reconstructed either using agnostic imaging algorithms or by direct fitting with model images from the general relativistic magnetohydrodynamic (GRMHD) simulated image library. The central brightness depression seen in the obtained image has been interpreted as the shadow cast by the central black hole owing to gravitational lensing of photons originating from the surrounding plasma and the overall image is consistent with the expected shadow of Kerr black hole in GR. The central compact radio source has been resolved as an asymmetric bright emission ring with an angular diameter of $42 \pm 3 \mu\text{as}$, wherein the asymmetry arises due to relativistic beaming of photons. Further, the shadow image was found to exhibit a deviation from circularity $\Delta C \leq 0.1$ and an axis ratio $\lesssim 4/3$ (Akiyama et al. 2019a,b,c). These observational constraints offer a clean gravitational test of the black-hole metric in the strong-field regime which we intend to employ to test the viability of black holes with an additional hair parameter in the Horndeski theory and then go on to measure its distinguishability from the Kerr metric.

In the present work we intend to probe the recently obtained (Walia et al. 2021) rotating black holes in Horndeski theory with an additional hair parameter h assuming the M87* as one and impose the astronomical constrains : (i) $\Delta C \leq 0.1$ (ii) $39 \mu\text{as} \leq \theta_d \leq 45 \mu\text{as}$ on the (M, a, h) parameter region of the black hole. Within the constrained parameter space, we carryout a systematic bias analysis to find out whether the various shadow observables of black holes in Horndeski theory and GR are distinguishable at the current 10% uncertainty of the EHT results; we take the shadow area A and oblateness D to define a cost function, reduced χ^2 , that we minimize over the parameter space ($a-h$) to determine whether it is large enough to distinguish the two theories of gravity in question with the cur-

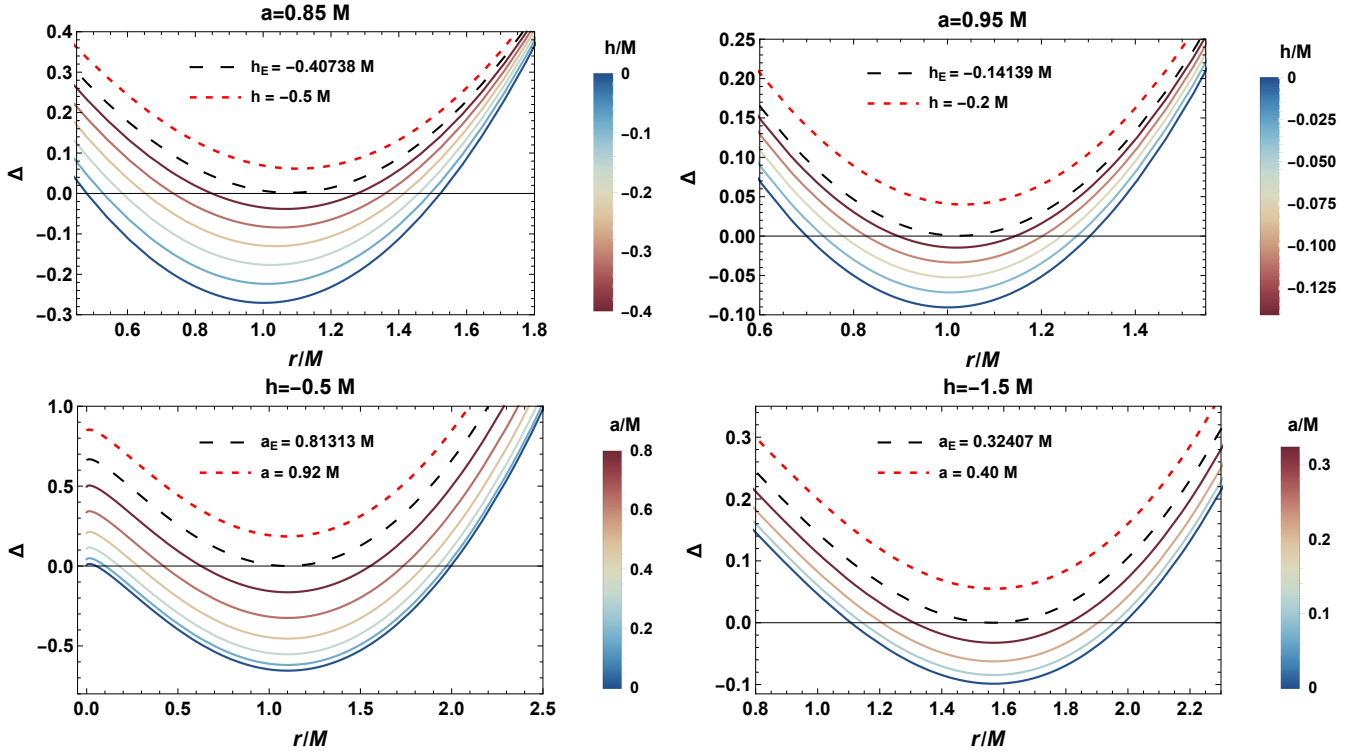


Figure 2. Horizons of the rotating Horndeski black holes are shown with varying hair parameter h (top) and spin a (bottom), compared with the Kerr black hole ($h = 0$ corresponding to bottom most solid curves).

rent resolution of the *EHT*. Thus in principle, the work would test the Kerr hypothesis within the current observational uncertainties of the *EHT* and in turn would place constraints on the parameters of the black hole and consequently on the underlying modified theory of gravity (MoG) as well.

2. ROTATING HAIRY BLACK HOLES IN HORNDESKI THEORY

Considering the action for a quartic scalar field ϕ in Horndeski theory

$$S = \int \sqrt{-g} \left\{ Q_2(\chi) + Q_3(\chi) \square \phi + Q_4(\chi) R + Q_{4,\chi} [(\square \phi)^2 - (\nabla^\mu \nabla^\nu \phi)(\nabla_\mu \nabla_\nu \phi)] \right\} d^4x, \quad (1)$$

where g is the determinant of the metric and R is the Ricci scalar and with the assumptions of finite energy of the scalar field in a volume, and vanishing radial component of 4-current j^ν at infinity, an exact static and spherically symmetric hairy black hole solution in the framework of Horndeski theory as been recently obtained by the authors in (Bergliaffa et al. 2021) as,

$$ds^2 = -A(r)dt^2 + \frac{1}{B(r)}dr^2 + r^2(d\theta^2 + \sin^2\theta d\varphi^2), \quad (2)$$

where, the 4-current,

$$j^\nu = \frac{1}{\sqrt{-g}} \frac{\delta S}{\delta(\phi_{,\mu})},$$

implies,

$$\begin{aligned} j^\nu = & -Q_{2,\chi} \phi^{,\nu} - Q_{3,\chi} (\phi^{,\nu} \square \phi + \chi^{,\nu}) \\ & - Q_{4,\chi} (\phi^{,\nu} R - 2R^{\nu\sigma} \phi_{,\sigma}) \\ & - Q_{4,\chi,\chi} \{ \phi^{,\nu} [(\square \phi)^2 - (\nabla_\alpha \nabla_\beta \phi)(\nabla^\alpha \nabla^\beta \phi)] \\ & + 2(\chi^{,\nu} \square \phi - \chi_{,\mu} \nabla^\mu \nabla^\nu \phi) \}, \end{aligned} \quad (3)$$

and thus varying the action (1) with respect to $g^{\mu\nu}$, the field equations

$$Q_4 G_{\mu\nu} = T_{\mu\nu}, \quad (4)$$

are obtained, where,

$$\begin{aligned} T_{\mu\nu} = & \frac{1}{2} (Q_{2,\chi} \phi_{,\mu} \phi_{,\nu} + Q_2 g_{\mu\nu}) + \frac{1}{2} Q_{3,\chi} (\phi_{,\mu} \phi_{,\nu} \square \phi \\ & - g_{\mu\nu} \chi_{,\alpha} \phi^{,\alpha} + \chi_{,\mu} \phi_{,\nu} + \chi_{,\nu} \phi_{,\mu}) - Q_{4,\chi} \left\{ \frac{1}{2} g_{\mu\nu} [(\square \phi)^2 \right. \\ & - (\nabla_\alpha \nabla_\beta \phi)(\nabla^\alpha \nabla^\beta \phi) - 2R_{\sigma\gamma} \phi^{,\sigma} \phi^{,\gamma}] - \nabla_\mu \nabla_\nu \phi \square \phi \\ & + \nabla_\gamma \nabla_\mu \phi \nabla^\gamma \nabla_\nu \phi - \frac{1}{2} \phi_{,\mu} \phi_{,\nu} R + R_{\sigma\mu} \phi^{,\sigma} \phi_{,\nu} \\ & \left. + R_{\sigma\nu} \phi^{,\sigma} \phi_{,\mu} + R_{\sigma\nu\gamma\mu} \phi^{,\sigma} \phi^{,\gamma} \right\} \\ & - Q_{4,\chi,\chi} \left\{ g_{\mu\nu} (\chi_{,\alpha} \phi^{,\alpha} \square \phi + \chi_{,\alpha} \chi^{,\alpha}) + \frac{1}{2} \phi_{,\mu} \phi_{,\nu} \times \right. \\ & (\nabla_\alpha \nabla_\beta \phi \nabla^\alpha \nabla^\beta \phi - (\square \phi)^2) - \chi_{,\mu} \chi_{,\nu} \\ & - \square \phi (\chi_{,\mu} \phi_{,\nu} + \chi_{,\nu} \phi_{,\mu}) \\ & \left. - \chi_{,\gamma} [\phi^{,\gamma} \nabla_\mu \nabla_\nu \phi - (\nabla^\gamma \nabla_\mu \phi) \phi_{,\nu} - (\nabla^\gamma \nabla_\nu \phi) \phi_{,\mu}] \right\}. \end{aligned} \quad (5)$$

The above expression reduces to the correct one in the case of the canonical action for the scalar field $\phi \equiv \phi(r)$ which is the source of the static and spherically symmetric geometry, described by the metric (2). Imposing conditions of finite energy of ϕ i.e., $E = \int_V \sqrt{-g} T_0^0 d^3x$ and a vanishing radial 4-current at infinity $j^r = 0$, and using the field equations (4), it follows that the metric components of (2) stand,

$$A(r) = B(r) = 1 - \frac{2M}{r} + \frac{h}{r} \ln\left(\frac{r}{2M}\right). \quad (6)$$

It can be easily seen that the solution Eq. (6), when $h \rightarrow 0$ would recover the Schwarzschild solution.

Recently, the authors in (Walia et al. 2021) using the Azreg-Aïnou's non-complexification procedure (Azreg-Aïnou 2014a,b) obtained the rotating counterpart of the hairy black hole (2) which apart from the mass (M) and spin (a) also depend on the hair parameter (h) which also gives potential deviation from the Kerr solution Kerr (1963). The rotating black holes in Horndeski theory written in the Boyer-Lindquist coordinates reads,

$$ds^2 = - \left[1 - \frac{2f}{\Sigma} \right] dt^2 + \frac{\Sigma}{\Delta} dr^2 + \Sigma d\theta^2 + \frac{A \sin^2 \theta}{\Sigma} d\phi^2 - \frac{4af \sin^2 \theta}{\Sigma} dt d\phi, \quad (7)$$

with $\Sigma = r^2 + a^2 \cos^2 \theta$,

$$2f = 2Mr - hr \ln\left(\frac{r}{2M}\right),$$

$$A = (r^2 + a^2)^2 - a^2 \Delta \sin^2 \theta,$$

$$\text{and } \Delta = r^2 + a^2 - 2Mr + hr \ln\left(\frac{r}{2M}\right), \quad (8)$$

The three parameter metric (7) further encompasses the family of spacetimes: *non-rotating Horndeski* ($a = 0, h \neq 0$), *Kerr* ($a \neq 0, h = 0$) and *Schwarzschild* ($a = 0, h = 0$). The axially symmetric spacetime (7) is asymptotically flat owing to the fact that the metric components crudely approach those of the Minkowski metric in spherical polar coordinates (in the limit $r \rightarrow \infty$), which has similarly been demonstrated for the Kerr metric (see, Ashtekar & Hansen 1978). Hairy black holes are well studied in literature viz., the stationary black hole solution with new global charges, which are not associated with Gauss law (Herdeiro & Radu 2015), e.g., black holes with procia hair (Herdeiro et al. 2016) or scalar hair (Herdeiro & Radu 2014; Gao & Xie 2021). A recent review on black holes with hair due to global charge can be found in (Herdeiro & Radu 2015). Without loss of generality we term the black holes (7) as

rotating Horndeski black holes having hair parameter h , which can be seen as a prototype non-Kerr metric with the Kerr mass M replaced by the mass function

$$m(r) = M - \frac{h}{2} \ln\left(\frac{r}{2M}\right).$$

At spacetime points where $\Sigma \neq 0$ and $g^{\alpha\beta} \partial_\alpha r \partial_\beta r = g^{rr} = \Delta = 0$, the metric (7) has coordinate singularity. The radial roots of

$$r^2 + a^2 - 2Mr + hr \ln\left(\frac{r}{2M}\right) = 0, \quad (9)$$

give the inner Cauchy horizon (r_-) and outer event horizon (r_+) radii for the allowed parameter space points (a, h) of the rotating hairy Horndeski black hole (7) (cf. Fig. 1). In the limit of vanishing hair parameter $h \rightarrow 0$, the equation (9) gives the horizons of the Kerr metric,

$$r_{\pm}^{Kerr} = M \pm \sqrt{M^2 - a^2}. \quad (10)$$

We depict the allowed parameter space ($a - h$) of the rotating hairy Horndeski black hole in Fig. 1, wherein, the shaded region demarcates all values of parameters $0 \leq a < a_E$ and $h_E < h \leq 0$ for which equation (7) has real roots. On the boundary (a_E, h_E) of the allowed parameter space (solid line in Fig. 1), we get an extremal black hole with degenerate horizons ($r_- = r_+$) and beyond this a naked singularity is obtained.

Fig. 2 depicts the horizon structure of the rotating Horndeski black holes where from it can be seen that, for a fixed value of spin a , there exists critical extremal value of hair parameter h_E and likewise there exists critical extremal value of spin a_E for given value of h , where $\Delta = 0$ has a double root. The rotating hairy Horndeski black hole exists when $a < a_E$ while for $a > a_E$ there is a naked singularity and the a_E depends on h , e.g., for $h = -0.5M, -1.5M$ respectively, $a_E = 0.81313M, 0.32407M$. Likewise, for a given spin a , the rotating hairy Horndeski black hole exists when $h > h_E$ while for $h < h_E$ there is a naked singularity. We find that the h_E depends on a , e.g., viz., for $a = 0.6M, 0.9M$ respectively, $h_E = -0.98328M, -0.27713M$.

As a generic property of axially symmetric spacetimes, the frame dragging effect in vicinity of the rotating Horndeski black holes (7) is caused by its non-zero off diagonal element i.e., $g_{t\phi}$. Due to this effect, a stationary observer outside the event horizon, moving with zero angular momentum with respect to an observer at spatial infinity rotates with the black hole with an angular velocity given by (Pugliese & Quevedo 2018)

$$\tilde{\omega} = \frac{d\phi}{dt} = -\frac{g_{t\phi}}{g_{\phi\phi}} = \frac{2ar(M - \frac{h}{2} \ln \frac{r}{2M})}{(r^2 + a^2)^2 - a^2 \Delta \sin^2 \theta}, \quad (11)$$

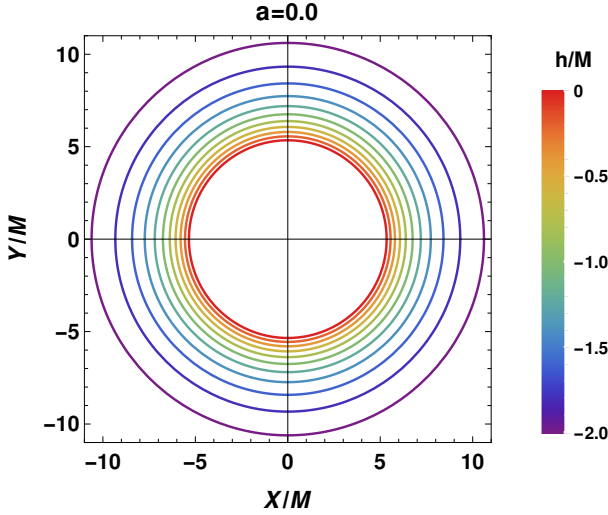


Figure 3. Shadow geometry of non-rotating Horndeski black holes ($a = 0$) with varying h . The concentric circular shadow silhouette are shown for equispaced h values. The shadow rings are sparsely spaced at higher values of h .

The velocity $\tilde{\omega}$ increases monotonically as the observer approaches the black hole and at the event horizon, the observer begins maximally co-rotating with a velocity equal to that of the black hole, which is given by,

$$\Omega = \tilde{\omega}|_{r=r_+} = \frac{2ar_+(M - \frac{h}{2} \ln \frac{r_+}{2M})}{(r_+^2 + a^2)^2}. \quad (12)$$

In the limit $h \rightarrow 0$,

$$\Omega^{Kerr} = \frac{2Mar_+}{(r_+^2 + a^2)^2} \quad (13)$$

corresponds to the angular velocity of Kerr black hole. The equation (13) shows that the surface of the black hole is rotating as a rigid body (Frolov & Frolov 2014) in a sense that each point of the horizon has the same angular velocity (as measured at infinity).

3. SPHERICAL ORBITS AND ANALYTICAL SHADOW STRUCTURE

The particle geodesics around the black hole while being a precursor to the study of phenomena such as strong field gravitational lensing, accretion process and shadow formation, carry more intrinsic significance in a sense that they bear imprint of the theory of gravity on which the spacetime is laid. We thus briefly introduce the spacetime symmetries of the stationary, axially symmetric black hole and study the photon geodesics thereon. The metric (7) having time translational and axisymmetric Killing vectors $\chi_{(t)}^\mu = \delta_t^\mu$ and $\chi_{(\phi)}^\mu = \delta_\phi^\mu$, have corresponding conserved quantities viz., the energy \mathcal{E} and axial component of angular momentum \mathcal{L} .

The two Killing vectors $\chi_{(t)}^\mu$ and $\chi_{(\phi)}^\mu$ would allow the separation of the t and ϕ equations. The Petrov type D of the spacetime, which accounts for Kerr's separability properties is implied from the existence of a non-apparent symmetry, the Killing-Yano 2-tensor; the conserved Carter constant \mathcal{Q} which is related to the Killing-Yano tensor field results in the separation of the r and θ equations (Chandrasekhar 1985). The additional integral of motion provided by Carter's constant makes the geodesic equations completely integrable and following Carter's approach we use the Hamilton-Jacobi equations to obtain four independent first order equations of photon motion (Frolov & Zelnikov 2011),

$$\Sigma \frac{dt}{d\lambda} = \frac{r^2 + a^2}{\Delta} (\mathcal{E}(r^2 + a^2) - a\mathcal{L}) - a(a\mathcal{E} \sin^2 \theta - \mathcal{L}), \quad (14)$$

$$\Sigma \frac{dr}{d\lambda} = \pm \sqrt{\mathfrak{R}(r)}, \quad (15)$$

$$\Sigma \frac{d\theta}{d\lambda} = \pm \sqrt{\Theta(\theta)}, \quad (16)$$

$$\Sigma \frac{d\phi}{d\lambda} = \frac{a}{\Delta} (\mathcal{E}(r^2 + a^2) - aL_z) - (a\mathcal{E} - \frac{\mathcal{L}}{\sin^2 \theta}), \quad (17)$$

where λ is the affine parameter. The radial and polar potential functions \mathfrak{R} and Θ are respectively given by (Chandrasekhar 1985),

$$\mathfrak{R} = \left((r^2 + a^2)E - aL_z \right)^2 - \Delta \left(\mathcal{K} + (aE - L_z)^2 \right) \quad (18)$$

$$\Theta = \mathcal{K} - \left(\frac{L_z^2}{\sin^2 \theta} - a^2 E^2 \right) \cos^2 \theta. \quad (19)$$

Here the conserved quantities \mathcal{L} and \mathcal{E} are the angular momentum and energy of the test particle, which are related with the Killing vector fields ∂_ϕ and ∂_t , respectively. Also, \mathcal{K} is the separability constant related to the Carter constant \mathcal{Q} through $\mathcal{Q} = \mathcal{K} + (aE - L_z)^2$ (Chandrasekhar 1985). Moreover, we introduce two energy re-scaled parameters,

$$\xi = \frac{\mathcal{L}}{\mathcal{E}}, \quad \eta = \frac{\mathcal{Q}}{\mathcal{E}^2}, \quad (20)$$

termed the critical parameters, which bring down the degree of of freedom in equations (14)-(17) from three to two, whereby, the photon motion around the stationary axisymmetric black hole is in essence determined independently by only the two critical parameters (20). The values of ξ and η result in three different classes of photon trajectories: *plunging*, *flyby* and *spherical*. For a spherical photon orbit (SPO) at radius r_p , we must have a radial turning point given by $\dot{r} = 0$, $\ddot{r} = 0$ which further imply, $\mathfrak{R} = 0$ and $\mathfrak{R}' = 0$ (see, Teo 2021) and thus using equation (18) we get the values of critical impact

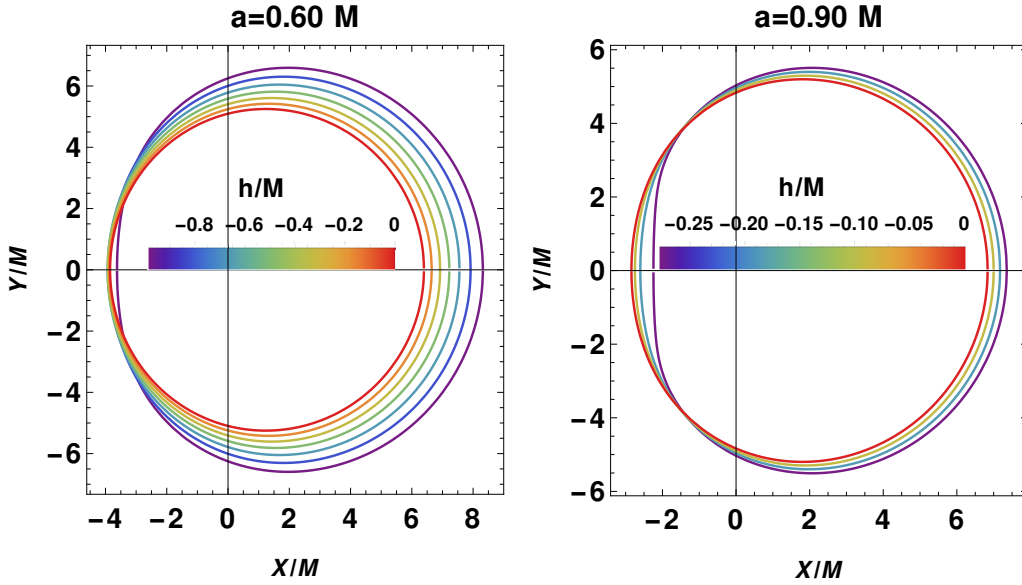


Figure 4. Shadow geometry of rotating Horndeski black holes with varying h for different spin parameters a . The maximum allowed value of the h used in the shadow construction is obtained from the black hole parameter space in Fig. 1 viz., $h = -0.9833M, -0.2771M$ for $a = 0.6M, 0.9M$ respectively.

parameters for SPOs in the rotating hairy Horndeski spacetime (7),

$$\xi_c = - \left[h(3r^2 - a^2) \log \left(\frac{Mr}{2} \right) - a^2(h - 2M - 2r) - r^2(h + 6M - 2r) \right] / \left[a \left(h \log \left(\frac{Mr}{2} \right) + h - 2M + 2r \right) \right] \quad (21)$$

$$\eta_c = -r^3 \left[2h \log \left(\frac{Mr}{2} \right) (4a^2 - 3r(h + 6M - 2r)) - 8a^2(h + 2M) + 9h^2 r \log^2 \left(\frac{Mr}{2} \right) + r(h + 6M - 2r)^2 \right] / \left[a^2 \left(h \log \left(\frac{Mr}{2} \right) + h - 2M + 2r \right)^2 \right]. \quad (22)$$

For the limiting value of hair parameter $h \rightarrow 0$, the equations (21) and (22) reduce to the critical impact parameters of the Kerr SPOs (Chandrasekhar 1985). The photon shell, is the region of a black hole spacetime containing bound null geodesics: while for the Schwarzschild black holes it is a 2-dimensional sphere with radius $3M$, for Kerr black hole a 3-dimensional spherical shell with (Johnson et al. 2020)

$$r_p^- \leq r_p \leq r_p^+, \quad (23)$$

$$r_p^\mp \equiv 2M \left[1 + \cos \left(\frac{2}{3} \arccos \left(\mp \frac{|a|}{M} \right) \right) \right] \quad (24)$$

where, r_p^\mp are respectively the prograde and the retrograde photon radii : $\eta = 0$, $\xi(r_p^\mp) \geq 0$. While a unique bound orbit passes through the equatorial annulus: $r_p^- \leq r \leq r_p^+$, $\theta = \pi/2$; on the boundaries $r = r_p^\pm$, the orbits are planar and confined to the equatorial plane

(Teo 2021). For the zero angular momenta photons, the overall direction of the orbits reverses at the intermediate value r_p^0 for which $\xi = 0$. Whereas, at generic points the spherical photons oscillate in the θ -direction between polar angles (Johnson et al. 2020),

$$\theta_\pm = \arccos(\mp \sqrt{u_\pm}), \quad (25)$$

with

$$u_\pm = \frac{r}{a^2(r-M)^2} \left[-r^3 + 3M^2r - 2a^2M \pm 2\sqrt{M\Delta(2r^3 - 3Mr^2 + a^2M)} \right]. \quad (26)$$

At the radius $r = r_p^0$, $\{\theta_-, \theta_+\} = \{0, \pi\}$ and the orbits can cross the poles. Thus the photon shell can be summarized as all spacetime points,

$$r_p^- \leq r \leq r_p^+, \quad \theta_- \leq \theta \leq \theta_+, \quad 0 \leq \phi < 2\pi, \quad -\infty \leq t \leq \infty$$

The bound geodesics are unstable i.e. at $r = r_p \in (r_p^-, r_p^+)$, the $\mathfrak{R}' \leq 0$ and a slight perturbation will result in an exponential divergence of the photon away from its spherical orbit. Slightly tighter orbits plunge into the black hole, while slightly larger orbits escape to infinity. The observed photon ring image arises from photons traveling on such ‘‘nearly bound’’ geodesics (Johnson et al. 2020).

3.1. Shadow structure

The critical curve \mathcal{C} (Bardeen 1973) or black hole shadow silhouette is a theoretical closed curve on the image plane of an observer defined by the locus of all

asymptotic arrival positions of unstable spherical photons that orbit the black hole arbitrarily many times before reaching the observer. The shape \mathcal{C} depends on the black hole parameters i.e. spin and other hairs and the observer inclination θ_0 (Afrin et al. 2021) relative to the spin axis, with the overall size scaled by the black hole mass M . In the limit of vanishing photon ring thickness, the photon ring reduces to the projection along the spherical null orbits in the equatorial plane of the black hole thus outlining the geometrical shadow silhouette of the black hole (Johannsen 2013) which we study, in the present scenario, as encoded by the rotating Horndeski black hole parameters a and h .

A distant observer viewing the black hole at inclination θ_0 relative to the spin axis will then see this asymptotic brightness enhancement at Cartesian screen coordinates given by (see, Bardeen 1973; Frolov & Zelnikov 2011):

$$\begin{aligned} X(r_p, r_0, \theta_0) &= \lim_{r_o \rightarrow \infty} \left(-r_o^2 \sin \theta_o \frac{d\phi}{dr} \right) \\ &= -\xi_c(r_p) \csc \theta_o, \\ Y(r_p, r_0, \theta_0) &= \lim_{r_o \rightarrow \infty} \left(r_o^2 \frac{d\theta}{dr} \right) \\ &= \pm \sqrt{\eta_c(r_p) + a^2 \cos^2 \theta_o - \xi_c(r_p)^2 \cot^2 \theta_o} \end{aligned} \quad (27)$$

Here, the projected spin direction on the observer's screen lies along the y -direction. The interior of this curve corresponds to the observer's line of sight into the black hole. Further for equatorial observer ($\theta_o = \pi/2$), equation (27) it simplifies to

$$\begin{aligned} X(r_p) &= -\xi_c(r_p), \\ Y(r_p) &= \pm \sqrt{\eta_c(r_p)}. \end{aligned} \quad (28)$$

Figure 3 depicts the parametric shadow silhouette of non-rotating hairy Horndeski black hole when viewed edge-on from the equatorial plane. For a non-rotating hairy Horndeski black hole ($a = 0$), the shadow is circular and has a radius smaller than the Schwarzschild radius of $\sqrt{X(r)^2 + Y(r)^2} = \sqrt{27}M$ (Synge 1966) with the hair parameter having a decremental effect on the shadow size. Furthermore, Fig. 4 depicts the shadow geometry for the rotating Horndeski black holes and as h deviates from $h = 0$, the shadow is displaced horizontally and flattens on the prograde photon side. This effect becomes most pronounced in the limit $h \rightarrow h_E$ and $\theta_0 \rightarrow \pi/2$ (a rotating maximally hairy Horndeski black hole viewed edge-on). Also, an interesting observation from Fig. 4 is that the influence of the h parameter on the D-shape shadow deformation is similar

to that caused by the spin a on the Kerr black hole's shadow. Hence, it is likely that the rotating Horndeski black holes for some parameters (a - h) may mimic the Kerr black hole shadow with a spin a^* .

4. ESTIMATION OF BLACK HOLE PARAMETERS

The first order approximation of the shadow shape is a circle with a radius equal to gravitationally lensed photon capture radius, which, for a given back ground spacetime, is determined by the distance and viewing angle of the observer apart from the mass of the central black hole (Tsukamoto et al. 2014). While the first order correction to the circular shadow shape occurs due to the black hole spin in Kerr spacetime, in MoGs the distortion for a given spin parameter may arise due to presence of additional hair as well (see Afrin et al. 2021; Cunha et al. 2015, 2019, for reference). For the rotating hairy Horndeski black hole (7), the onset of a discernible dent in the prograde shadow region with the increase in the h can be seen from Fig. 3.

Hitherto we have seen how the black hole parameters leave signatures in the shadow silhouette which may in turn directly give a prescription to test MoGs using the shadow shape and size (Kumar & Ghosh 2020a; Tsukamoto et al. 2014; Hioki & Maeda 2009). But inversely, the black hole shadow has been deployed to estimate the parameters of the central black hole by a simple contour intersection method (Hioki & Maeda 2009; Kumar & Ghosh 2020a) which can thus numerically measure additional hair parameters from observed shadow (Afrin et al. 2021). One observable of the shadow can in essence determine only one parameter of the background metric and it was demonstrated that the Hioki-Maeda (Hioki & Maeda 2009) observable, distortion parameter δ_s , carries degeneracy with respect to the spin and other deformation (or hair) parameters and thus to assess possible deviations from the Kerr solution, one has to observe more than one quantity to test the Kerr black hole hypothesis (see, Tsukamoto et al. 2014).

Also, it was found that distinguishing Kerr and non-Kerr black holes from the sole observation of the shadow is extremely difficult as an accurate mass to distance ratio of the black hole would be necessary for the estimation of its other parameters and a combination of the measurement of the shadow with possible accurate radio observations of a pulsar in a compact orbit around the supermassive black holes could be a more propitious strategy to test the Kerr hypothesis (Tsukamoto et al. 2014). Furthermore, it was shown in multiple studies that the δ_s alongside the shadow radius R_s (Hioki & Maeda 2009) demand some specific symmetry in the shadow shape and thus may

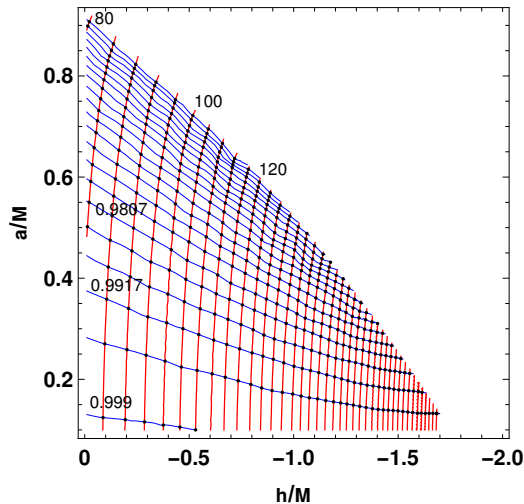


Figure 5. Contour plots of the observables A/M^2 and D in the rotating hairy Horndeski black hole parameter space $(a/M, h/M)$. Solid red curves correspond to 40 equispaced constant contours of A/M^2 ranging from 80 to 240 while 20 constant contours of D ranging from 0.926 to 0.999 are shown by the blue solid curves. The intersection points of the $A - D$ lines are shown by the black points.

Table 1. Numerically estimated values of rotating hairy Horndeski black hole parameters a/M and h/M from shadow observables A and D .

A/M^2	D	a/M	h/M
84	0.94060	0.8119	-0.1090
92	0.95520	0.6816	-0.2899
100	0.96980	0.5484	-0.4424
120	0.98805	0.3071	-0.7545
192	0.99535	0.1383	-1.4350

not be efficient in some MoGs as well as for noisy data (Abdujabbarov et al. 2015). Thereafter, Kumar and Ghosh (Kumar & Ghosh (2020a)), proposed estimating the black hole parameters from haphazard shadow shapes using two new shadow observables that we introduce briefly below and subsequently use to estimate the parameters associated with the rotating hairy Kerr black holes (7). We assume an equatorial ($\theta_0 = \pi/2$) observer for estimating the black hole parameters.

4.1. Shadow Observables

The fast spinning axially symmetric astrophysical black holes do not cast a circular shadow when seen at large viewing angles away from the poles (Frolov & Zelnikov 2011). The prograde region of the shadow is dented leaving the top, bottom as well as ret-

rograde region. For the approximate characterization of the non-circular shadow, the deviation of the shadow shape S from a reference circle S' is considered. The reference circle S' coincides at the top (X_t, Y_t) , bottom (X_b, Y_b) and right $(X_r, 0)$ edges with the shadow contour (Ghosh et al. 2020), while $(X'_l, 0)$ and $(X_l, 0)$ are respectively the points where the reference circle and leftmost edge of the shadow contour intersects the horizontal axis. To relegate the observed shadow to the any particular theory of the underlying gravity, we collate a pair of shadow observables: the shadow area A and oblateness D . The shadow area (A) is given by (Kumar & Ghosh 2020a; Tsupko 2017),

$$A = 2 \int Y(r_p) dX(r_p) = 2 \int_{r_p^-}^{r_p^+} \left(Y(r_p) \frac{dX(r_p)}{dr_p} \right) dr_p, \quad (29)$$

whereas, the oblateness (D) can be written as (Kumar & Ghosh 2020a),

$$D = \frac{X_r - X_l}{Y_t - Y_b}. \quad (30)$$

4.2. Estimation of parameters

Evidently from the shadow structure seen in Fig. (4) both the parameters a and h have profound impact on the shadow area as well as the oblateness. Interestingly, there maybe possible degeneracy of the A and D observables in the a and h in the sense that two or more combinations of the black hole parameters ($a-h$) may give the same area A_1 and/or the same oblateness D_1 . We explore these possibilities by plotting the constant contour lines of the observables A and D in the $(a-h)$ plane as shown in Fig. 5. From the Fig. 5 we note the following,

1. A contour of a given observable (A or D) gives one-to-one correspondence between a and h parameters.
2. The contours of the two different observables (A and D) intersect at unique points.

From the first observation it can be inferred that both the shadow observables A and D are non-degenerate in parameters (a, h) if at least one of the two parameters are fixed. Also, the observables are degenerate for an infinite number of unique parameter points lying on a given constant contour curve. Interestingly, from the second observation we surmise that from each intersection point (the black points in Fig. 5) of a particular A and D contour line, one can uniquely determine the parameters a and h of the central black hole. We estimate

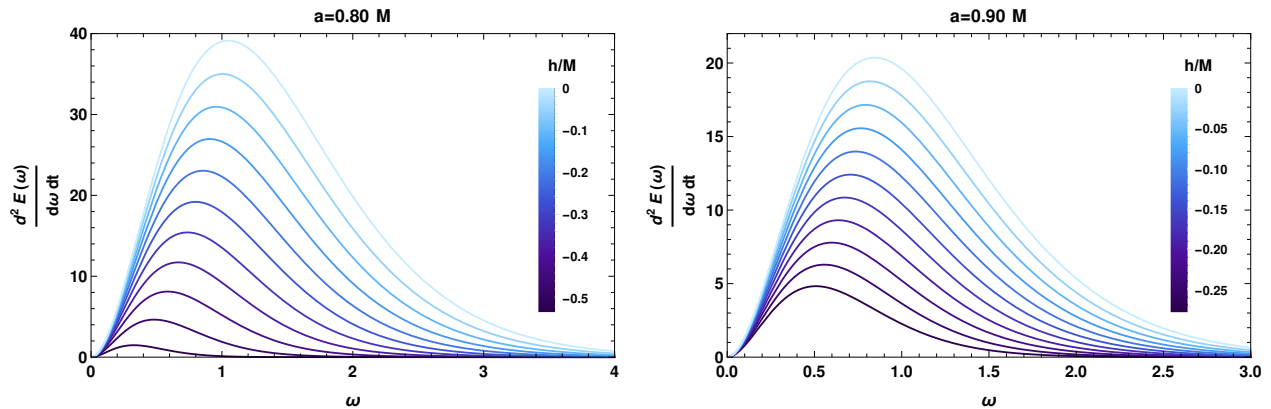


Figure 6. Evolution of the emission rate with the frequency ω for different values of parameter h and α for the rotating Horndeski black holes.

the parameters of the rotating hairy Horndeski black hole (7) that we tabulate in Table 1. Thus, with any astronomically observed data set ($A-D$) for e.g. the *EHT* results of the M87* (Akiyama et al. 2019a,b,c) or the future next generation *EHT* (*ngEHT*) (Raymond et al. 2021) with more accurate observation (upto 345GHz observational frequency and new telescope sites) can pin down the parameters a and h to a precision directly determined by the precision of the observation.

4.3. Energy emission

The black hole shadows apart from serving as a tool to probe and constrain various theories of gravity (Kumar & Ghosh 2020a,b; Afrin et al. 2021) can lead to the theoretical prediction of various interesting astronomical phenomena as well. In this paper, we intend to study the energy emission rate by the rotating Horndeski black holes. To an asymptotically far away observer, the shadow of an axially symmetric black hole corresponds to a high energy absorption cross-section, which oscillates around a constant limiting value σ_{lim} corresponding to a spherically symmetric black hole. The σ_{lim} is the same as the geometrical cross-section of the photon sphere of the central black hole and it takes the form (Wei & Liu 2013),

$$\sigma_{lim} \approx \pi R_s^2, \quad (31)$$

where R_s designates approximately the size of the shadow and is defined as (Hioki & Maeda 2009)

$$R_s = \frac{(X_t - X_r)^2 + Y_t^2}{2|X_r - X_t|}. \quad (32)$$

The energy emission rate a rotating black hole is given by (Wei & Liu 2013),

$$\frac{d^2 E(\omega)}{d\omega dt} = \frac{2\pi^2 R_s^2}{e^{\omega/T} - 1} \omega^3, \quad (33)$$

where ω is photon frequency and T is the Hawking temperature at event horizon r_+ of black hole and for the rotating Horndeski black holes (7) it becomes,

$$T = \frac{1}{2\pi(a^2 + r_+^2)} (h(a^2 - r_+^2) \log\left(\frac{Mr_+}{2}\right) + a^2(h - 2M) + r_+^2(h + 2M)). \quad (34)$$

Interestingly, the Hawking temperature of the rotating Horndeski black holes depends on the parameters a as well as on h and in the limit $h \rightarrow 0$ reduces to the Hawking temperature of the Kerr black hole. In Fig. 6, we illustrate the behaviour of the energy emission rate of rotating Horndeski black holes against the photon frequency ω for various values of parameter h for two different values of a . The emission rate peak decreases from that of the Kerr value ($h = 0$ shown by the topmost curve in Fig. 6) with an increase in h and shifts to a lower value of ω with the increase in a .

5. CONSTRAINTS FROM *EHT*

The *EHT* collaboration (Akiyama et al. 2019b,a,c) by direct studies of the event horizon shadow of the SMBH M87* via electromagnetic waves obtained the size, asymmetry, brightness contrast, and circularity of the reconstructed images and geometric models to infer that the images of M87* are associated with strongly lensed synchrotron photons from the vicinity of a Kerr black hole which thus implied the non-violation of the Kerr hypothesis. But the results could not rule out alternatives to black holes in GR as any compact object with unstable circular photon orbits can cast a shadow (Mizuno et al. 2018). It has been shown in previous studies that while the Kerr metric remains a solution in some alternative theories of gravity (Barausse & Sotiriou 2008; Psaltis et al. 2008), non-Kerr black hole solutions do exist in several MoGs (Berti et al. 2015). Thus we now use the *EHT* con-

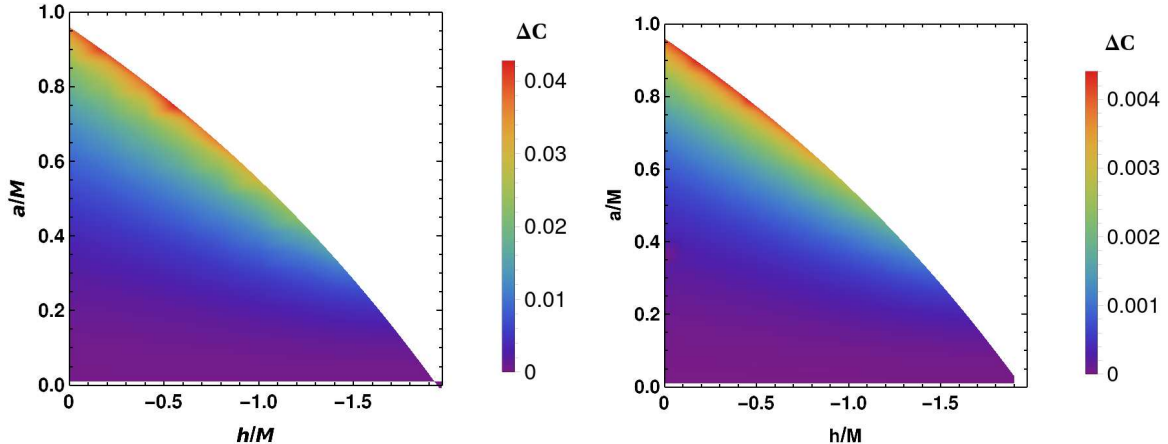


Figure 7. Circularity deviation observable ΔC for rotating hairy Horndeski black hole shadows as a function of parameters (a/M and h/M) in agreement with the *EHT* observations of the M87* black hole, $\Delta C \leq 0.1$, is satisfied for the entire parameter space (a/M and h/M). The parameters of M87* used are $M = 6.5 \times 10^9 M_\odot$ and $d = 16.8 \text{Mpc}$. The inclination angle is $\theta_0 = 90^\circ$ (left) and $\theta_0 = 17^\circ$ (right). The white region is forbidden for (a/M and h/M).

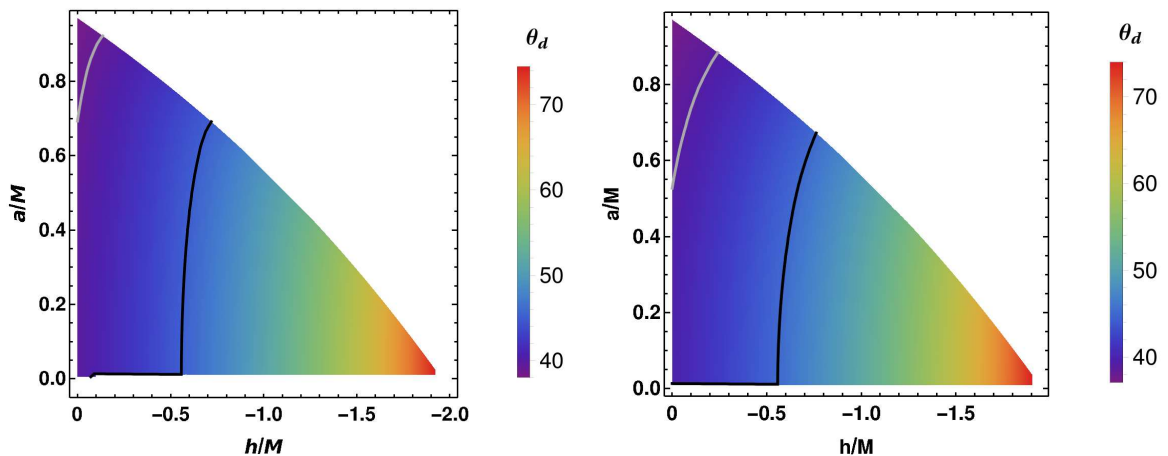


Figure 8. Angular diameter observable θ_d for rotating hairy Horndeski black hole shadows as a function of parameters (a/M and h/M). The gray and black solid curves correspond to $\theta_d = 39 \mu\text{as}$ and $\theta_d = 45 \mu\text{as}$ respectively within 1σ region of the measured angular diameter, $\theta_d = 42 \pm 3 \mu\text{as}$, of the M87* black hole as reported by the *EHT*. The mass and distance of M87* used are $M = 6.5 \times 10^9 M_\odot$ and $d = 16.8 \text{Mpc}$ respectively. The inclination angle is $\theta_0 = 90^\circ$ (left) and $\theta_0 = 17^\circ$ (right). The white region is forbidden for (a/M and h/M).

straints on two shadow observables : deviation from circularity $\Delta C \leq 10\%$ and $\theta_d = 42 \pm 3 \mu\text{as}$ to constrain the parameters a and h of the rotating Horndeski black holes (7) to be consistent with the M87* image within 1σ confidence. Thereon, in the next section, we will do a systematic bias analysis between the rotating Horndeski black holes and the Kerr black hole within this constrained parameter space (a - h) to test the distinguishability and possibility of testing GR against the Horndeski theory.

To use the above constraints, the shadow is compared with a reference circle (Hioki & Maeda 2009) such that, the reference circle coincides at the top (X_t, Y_t), bottom (X_b, Y_b) and right ($X_r, 0$) edges with the shadow contour (Ghosh et al. 2020), with ($X'_l, 0$) and ($X_l, 0$) being respectively the points where the reference circle and leftmost edge of the shadow contour intersects the horizontal axis. The boundary of the black hole shadow is outlined by the polar coordinates $(R(\varphi), \varphi)$, with origin at the shadow centre (X_c, Y_c) such that $X_c = (X_r - X_l)/2$ and $Y_c = 0$. The average shadow radius \bar{R} can be writ-

ten as (Bambi et al. 2019)

$$\bar{R}^2 = \frac{1}{2\pi} \int_0^{2\pi} R^2(\varphi) d\varphi, \quad (35)$$

where

$$R(\varphi) = \sqrt{(X - X_c)^2 + (Y - Y_c)^2}$$

and $\varphi \equiv \tan^{-1} \left(\frac{Y}{X - X_c} \right)$.

Here, φ is the polar angle between the x-axis of the image plane and the vector connecting the centre (X_c, Y_c) to a point (X, Y) lying on the boundary of the shadow. The circularity deviation ΔC is defined in terms of root-mean-square distance from an average radius as, (Bambi et al. 2019)

$$\Delta C(a, h) = \frac{1}{\bar{R}} \sqrt{\frac{1}{2\pi} \int_0^{2\pi} (R(\varphi) - \bar{R})^2 d\varphi}, \quad (36)$$

The ΔC quantifies deviation from a perfectly circular shadow such that, for non-spinning black hole $\Delta C = 0$ (refer to Fig. 3). Furthermore, the angular diameter of the shadow θ_d (Kumar & Ghosh 2020b) can be defined as

$$\theta_d = 2 \frac{R_a}{d}, \quad R_a = \sqrt{A(a, h)/\pi}, \quad (37)$$

where R_a is the shadow areal radius. The θ_d together with the ΔC will be useful to perform a comparison between the theoretical predictions for hairy Kerr BH shadows and the *EHT* observations (Bambi et al. 2019). Evidently, from equations (36) and (37) both the ΔC and θ_d depend on the black hole parameters. We presuppose the M87* a rotating hairy Horndeski black hole, calculate ΔC and θ_d for metric (7) and use the *EHT* observational result $\Delta C \leq 0.1$ and $39\mu\text{as} \leq \theta_d \leq 45\mu\text{as}$ to put constraints on the a and h .

The calculation of the θ_d apart from the a and h would also require a precise measurement of mass M and distance d of the M87* from earth. The mass of the M87* could be measured as $M = 6.5 \pm 0.2|_{\text{stat}} \pm 0.7|_{\text{sys}} \times 10^9 M_\odot$ (Roelofs et al. 2021) which is consistent with the mass obtained earlier using stellar dynamics. We thus take the $M = 6.5 \times 10^9 M_\odot$ and $d = 16.8$ Mpc as estimated by the *EHT* (Akiyama et al. 2019b,a,c). Also, taking into consideration the orientation of the magnetohydrodynamic relativistic jets in M87* image, the inclination angle (with respect to observational line of sight) is estimated to be 17° (Craig Walker et al. 2018). But the shadow is maximally deformed only at very high inclination, viz., $\theta_0 \approx 90^\circ$. Thus we carry out our calculations at both $\theta_0 = 90^\circ$ and $\theta_0 = 17^\circ$ observation angles.

The Fig. (7) shows a density plot of the ΔC in the parameter space (a - h) of the rotating Horndeski black holes (7) within the allowed region as demonstrated in Fig. 1. We find that the 1σ bound of the current *EHT* observations, $\Delta C \leq 0.1$ is satisfied for the entire parameter region (a - h) at both $\theta_0 = 90^\circ$ and $\theta_0 = 17^\circ$ and no upper or lower bounds can be placed on the parameters of the black hole (7).

We make a similar density plot of the θ_d in the parameter space (a - h) of the rotating Horndeski black holes (7) as shown in the Fig. 8 and interestingly, the *EHT* bounds $39\mu\text{as} \leq \theta_d \leq 45\mu\text{as}$ delineates only a limited parameter space bounded by the $\theta_d = 39\mu\text{as}$ (the gray line in Fig. 8) and $\theta_d = 45\mu\text{as}$ (the black line in Fig. 8) contours. Thus the astronomical observable θ_d puts strong upper limits on both a and h parameters of the rotating Horndeski black holes (7) within the 10% observational uncertainty of the *EHT* results (Akiyama et al. 2019b,a,c). Also, we must point out that the accordant parameter space (a - h) is more constricted at $\theta_0 = 17^\circ$ than at $\theta_0 = 90^\circ$. Thus the remarkable consistency of the rotating Horndeski black holes (7) with the M87* observations at an infinite number of possible parameter points (a, h) within the constrained parameter space elucidates the fact that they can be strong candidates for astrophysical black holes and thereby the Horndeski gravity if distinguishable from the GR would put the Kerr hypothesis to an astrophysical test.

6. SYSTEMATIC BIAS ANALYSIS

In the previous section, we demonstrated how the current *EHT* bounds on the black hole observables demarcate consistent parameters (a - h) of the rotating Horndeski black holes wherein the Horndeski theory is astrophysically viable. We study next, whether the rotating Horndeski black holes (7) can be distinguished from the Kerr black hole within its accordant parameter space (a - h) obtained in the previous section. To determine the possible degeneracy of the rotating hairy Horndeski black hole shadows and the shadows of Kerr black hole, we carry out a systematic bias analysis between an injected Kerr shadow and simulated shadows of rotating Horndeski black holes as models to fit with the injection. For a known mass-to-distance ratio M/d of the black hole and a fixed observer position (r_o, θ_o) , the injected shadow solely depends on the injected Kerr spin parameter a^* , whereas model shadows depend on both spin a and hair h of the metric (7). This hair parameter can significantly alter the shape and size of shadows of the rotating Horndeski black holes as visible from Fig. 4. To quantify the possible deviations of the shadow geometry

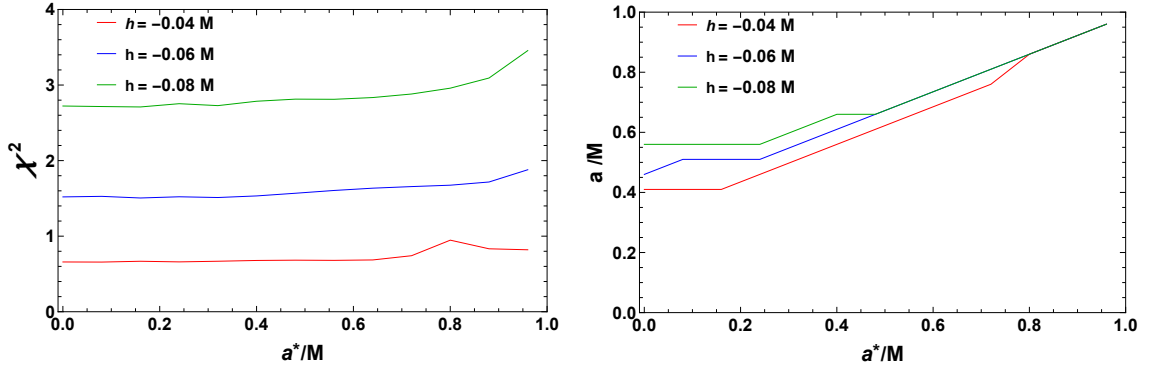


Figure 9. The minimized χ^2 (*left*) and extracted spin (*right*) of the best-fit rotating hairy Horndeski black hole model as a function of injected Kerr spin a^* . The reduced $\chi^2 \leq 1$ for very low negative values of the hair parameter h .

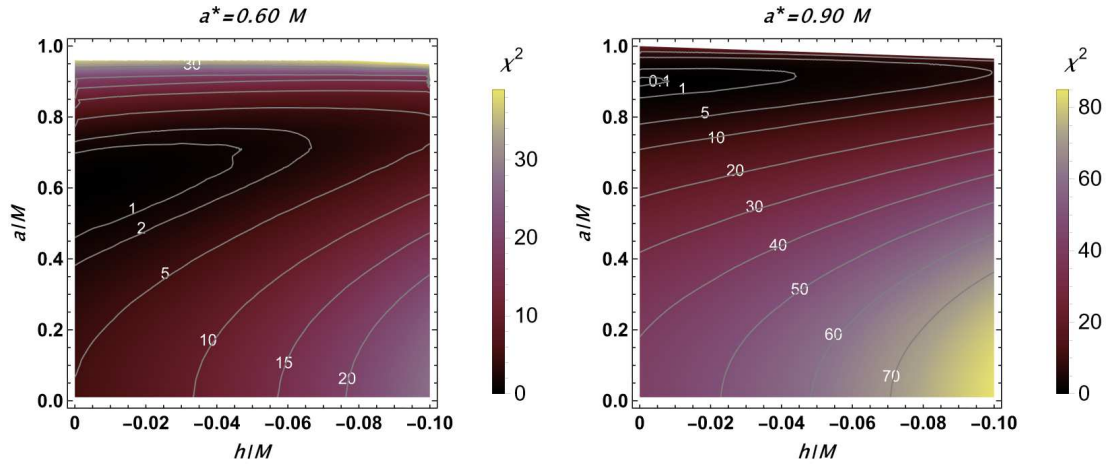


Figure 10. The reduced χ^2 between the rotating hairy Horndeski black hole and the Kerr black hole in the parameter space $(a/M - h/M)$ of the former, for different injected Kerr spin values $a^* = 0.60M$ (*left*), $0.90M$ (*right*). In the region bounded within the $\chi^2 = 1$ contours, the rotating hairy Horndeski black hole cannot be distinguished from the Kerr black hole from the present resolution of the *EHT* observations.

of the model from the injection we adopt the shadow observables A and D from equations (29) and (30) which over a given black hole model parameter space $(a-h)$ uniquely characterize its shadow.

To carry out the systematic bias analysis we calculate the reduced χ^2 between the model and the injection given by,

$$\chi^2(a, h, a^*) = \frac{1}{2} \sum_{i=1}^2 \left[\frac{\alpha^i(a, h) - \alpha_K^i(a^*)}{\sigma_i} \right]^2, \quad (38)$$

where, $\alpha^i \equiv \{A, D\}$ are the shadow observables. We consider the standard deviation σ_i as 10% of the range of each observable α^i , which is the current uncertainty in the observational measurements of the EHT (Akiyama et al. 2019a,b,c). For a given value of model parameter h , the reduced χ^2 between the model and the injection is minimized and the corresponding best-

fit value of the model spin a is extracted for each value of the injected spin a^* . In this model fitting procedure, the nonzero values of χ^2 quantify the departure of rotating hairy Horndeski black hole shadows from that of Kerr black hole shadows, such that for $\chi^2 \leq 1$ the rotating hairy Horndeski black hole shadow is degenerate with the Kerr shadow and the two are indistinguishable within the current observational uncertainties. Whereas $\chi^2 > 1$ signifies that the two shadow observations are astrophysically discernible, GR can be tested against the background MoG viz. the Horndeski gravity.

In Fig. 9 both the minimized χ^2 (*left* panel) and the extracted spin a (*right* panel) are plotted for different values of h . The Fig. 9 explicates that the minimized χ^2 increases with the increase in the h parameter which is expected a priori as the increase in parameter h will induced deviations from the Kerr observables. The $\chi^2 < 1$ for a very small value $h = -0.04M$ (viz., the red line in

the left panel of Fig. 9) for which the rotating Horndeski black holes are indistinguishable from the Kerr black hole for any all spin values a^* with the current observational accuracy of the *EHT*. Also for all h values the χ^2 increases with the increase in the a^* which implies that distinguishability increases and the near maximally rotating Kerr black hole can be easily tested against the rotating Horndeski black holes (7). Furthermore, from the right panel of Fig. 9 it can be seen that the best fit spin a for a given injected a^* increases with the increase in h thus implying that the black holes (7) with higher h must spin faster to resemble the Kerr black hole shadow. Also, one can see that at higher injected spin a^* (near extremally rotating Kerr black hole), the extracted spins a for all values of h take the same value. In Fig. 10, density plot of $\chi^2(a, h, a^*)$ is shown in the parameter space (a - h) of the model black hole (7) for two different injected spins $a^* = 0.6M, 0.9M$. One can observe that the $\chi^2 \leq 1$ is region bounded by the $\chi^2 = 1$ contour line demarcates a region with very low h values and with values of a close to a^* . Outside the $\chi^2 = 1$ contour, the deviation in observed shadow introduced by the Horndeski gravity is large enough to be observable and thus there is a possibility to put constraints on the parameters of the metric (7). In our current analysis (c.f. Fig. 10) we examine the behaviour of the $\chi^2(a, h, a^*)$ with $h \in [0, -0.1]$ to confine within the astronomical upper bound on the h as obtained from Fig. 8.

Thus, we have explored the possibility that within the parameter space (a - h) consistent with the M87* observations, whether the deviation in the shadow introduced by Horndeski gravity is large enough to be observable astrophysically. We found that indeed within the accordant parameter space, the systematic bias (reduced χ^2) of the the astrophysical observables of the Horndeski theory and the GR black holes is large enough to discern the two theories and it is possible to test GR against the Horndeski gravity at the current observational resolution of the *EHT*.

7. CONCLUSIONS

In this paper, we explored the prospects of astrophysical tests of the *Kerr hypothesis* and thus the viability of rotating black holes in MoGs like the Horndeski theory using the *EHT* observations of the M87* at its current resolution and observational uncertainty. The rotating Horndeski black holes that we studied, alongside mass M and spin a , have an additional hair parameter h and the analytic study of the Cauchy and event horizons reveal that the parameter h reduces the size of the horizon radii than those of the Kerr black hole's. Furthermore, using the first order photon geodesic equations, we ana-

lytically plot the shadow silhouette of the rotating hairy Kerr black holes and their non-rotating counterparts and find that the effect of the h parameter incremental on the shadow size which is contrary to many modified theory black holes wherein, the shadows are smaller than the Kerr shadow Interestingly, the h is found to incur deformations in the shadow shape and the dent increases with the increase in h for a given a . The shadow deformation is similar to that caused by the spin in Kerr black holes and thus a degeneracy between the shadow formed by rotating Horndeski black holes with parameter (a, h) and that casted by the Kerr black hole with some spin a^* is surmised.

Using the *EHT* observations of the M87* viz., $M = 6.5 \times 10^9 M_\odot$, $d = 16.8$ Mpc, $\Delta C \leq 0.1$ and $\theta_d = 42 \pm 3 \mu as$ we constrained the rotating hairy Horndeski black hole shadow observables ΔC and θ_d to find that while the $\Delta C \leq 0.1$ for the entire parameter space (a - h), the $39 \mu as \leq \theta_d \leq 45 \mu as$ puts tight upper bounds on both a and h and the consistent parameter space (a - h) is only a small portion of the entire allowed region and moreover it is more constricted at $\theta_0 = 17^\circ$ than at $\theta_0 = 90^\circ$ inclination. Thus we find that within the 1σ confidence level, the current *EHT* observations endorse the rotating Horndeski black holes as viable astrophysical candidate of the M87*.

Within the concordant parameter space (a - h) obtained from the current M87* bounds, a systematic bias analysis is carried out with the observables A and D of stimulated analytical shadows of the rotating Horndeski black holes as model and that of the Kerr black hole as the injection and the minimized reduced χ^2 is obtained for each injected Kerr spin $a^* \in [0, 1M)$ alongside the best-fit spin a for different h values of the rotating hairy Horndeski. We arrive at a very interesting observation that the $\chi^2 > 1$ for a large parameter space (a - h) within the $\theta_d = 42 \pm 3 \mu as$ M87* bounds which clearly suggests that the rotating Horndeski black holes are astronomically distinguishable from the Kerr black hole even at the present resolution of the *EHT* with a precise measurement of the a and h parameters along side the mass-to-distance ration M/d and the angle of observation. Thus our present work motivates the testing of the Horndeski gravity against the GR with astronomical probes like the *EHT* (Akiyama et al. 2019a,b,c), *ngEHT* (Raymond et al. 2021) and Event Horizon Imager(EHI) space VLBI array (Roelofs et al. 2021).

ACKNOWLEDGEMENTS

S.G.G. would like to thank SERB-DST for the ASEAN project IMRC/AISTDF/CRD/2018/000042.

M.A. is supported by DST-INSPIRE Fellowship, Department of Science and Technology, Govt. of India

REFERENCES

- Abbott, B. P., et al. 2016, *Phys. Rev. Lett.*, 116, 061102, doi: [10.1103/PhysRevLett.116.061102](https://doi.org/10.1103/PhysRevLett.116.061102)
- Abdujabbarov, A. A., Rezzolla, L., & Ahmedov, B. J. 2015, *Mon. Not. Roy. Astron. Soc.*, 454, 2423, doi: [10.1093/mnras/stv2079](https://doi.org/10.1093/mnras/stv2079)
- Afrin, M., Kumar, R., & Ghosh, S. G. 2021, *Mon. Not. Roy. Astron. Soc.*, 504, 5927, doi: [10.1093/mnras/stab1260](https://doi.org/10.1093/mnras/stab1260)
- Akiyama, K., et al. 2019a, *Astrophys. J. Lett.*, 875, L4, doi: [10.3847/2041-8213/ab0e85](https://doi.org/10.3847/2041-8213/ab0e85)
- . 2019b, *Astrophys. J. Lett.*, 875, L1, doi: [10.3847/2041-8213/ab0ec7](https://doi.org/10.3847/2041-8213/ab0ec7)
- . 2019c, *Astrophys. J. Lett.*, 875, L6, doi: [10.3847/2041-8213/ab1141](https://doi.org/10.3847/2041-8213/ab1141)
- Anabalón, A., Cisterna, A., & Oliva, J. 2014, *Phys. Rev. D*, 89, 084050, doi: [10.1103/PhysRevD.89.084050](https://doi.org/10.1103/PhysRevD.89.084050)
- Anderson, J. D., Laing, P. A., Lau, E. L., et al. 2002, *Phys. Rev. D*, 65, 082004, doi: [10.1103/PhysRevD.65.082004](https://doi.org/10.1103/PhysRevD.65.082004)
- Ashtekar, A., & Hansen, R. O. 1978, *J. Math. Phys.*, 19, 1542, doi: [10.1063/1.523863](https://doi.org/10.1063/1.523863)
- Azreg-Aïnou, M. 2014a, *Phys. Rev. D*, 90, 064041, doi: [10.1103/PhysRevD.90.064041](https://doi.org/10.1103/PhysRevD.90.064041)
- . 2014b, *Eur. Phys. J. C*, 74, 2865, doi: [10.1140/epjc/s10052-014-2865-8](https://doi.org/10.1140/epjc/s10052-014-2865-8)
- Bambi, C., Freese, K., Vagnozzi, S., & Visinelli, L. 2019, *Phys. Rev. D*, 100, 044057, doi: [10.1103/PhysRevD.100.044057](https://doi.org/10.1103/PhysRevD.100.044057)
- Barausse, E., & Sotiriou, T. P. 2008, *Phys. Rev. Lett.*, 101, 099001, doi: [10.1103/PhysRevLett.101.099001](https://doi.org/10.1103/PhysRevLett.101.099001)
- Bardeen, J. M. 1973, in *Les Houches Summer School of Theoretical Physics: Black Holes*
- Bergliaffa, S. E. P., Maier, R., & Silvano, N. d. O. 2021, <https://arxiv.org/abs/2107.07839>
- Berti, E., et al. 2015, *Class. Quant. Grav.*, 32, 243001, doi: [10.1088/0264-9381/32/24/243001](https://doi.org/10.1088/0264-9381/32/24/243001)
- Bhattacharya, S., & Chakraborty, S. 2017, *Phys. Rev. D*, 95, 044037, doi: [10.1103/PhysRevD.95.044037](https://doi.org/10.1103/PhysRevD.95.044037)
- Brihaye, Y., Cisterna, A., & Erices, C. 2016, *Phys. Rev. D*, 93, 124057, doi: [10.1103/PhysRevD.93.124057](https://doi.org/10.1103/PhysRevD.93.124057)
- Brito, F. A., & Santos, F. F. 2020, *EPL*, 129, 50003, doi: [10.1209/0295-5075/129/50003](https://doi.org/10.1209/0295-5075/129/50003)
- Carter, B. 1971, *Phys. Rev. Lett.*, 26, 331, doi: [10.1103/PhysRevLett.26.331](https://doi.org/10.1103/PhysRevLett.26.331)
- Chandrasekhar, S. 1985, *The mathematical theory of black holes*
- Charmousis, C., Kolyvaris, T., Papantonopoulos, E., & Tsoukalas, M. 2014, *JHEP*, 07, 085, doi: [10.1007/JHEP07\(2014\)085](https://doi.org/10.1007/JHEP07(2014)085)
- Cisterna, A., Delsate, T., Ducobu, L., & Rinaldi, M. 2016, *Phys. Rev. D*, 93, 084046, doi: [10.1103/PhysRevD.93.084046](https://doi.org/10.1103/PhysRevD.93.084046)
- Craig Walker, R., Hardee, P. E., Davies, F. B., Ly, C., & Junor, W. 2018, *Astrophys. J.*, 855, 128, doi: [10.3847/1538-4357/aaafcc](https://doi.org/10.3847/1538-4357/aaafcc)
- Cunha, P. V. P., Herdeiro, C. A. R., & Radu, E. 2019, *Universe*, 5, 220, doi: [10.3390/universe5120220](https://doi.org/10.3390/universe5120220)
- Cunha, P. V. P., Herdeiro, C. A. R., Radu, E., & Runarsson, H. F. 2015, *Phys. Rev. Lett.*, 115, 211102, doi: [10.1103/PhysRevLett.115.211102](https://doi.org/10.1103/PhysRevLett.115.211102)
- Damour, T., & Esposito-Farese, G. 1992, *Class. Quant. Grav.*, 9, 2093, doi: [10.1088/0264-9381/9/9/015](https://doi.org/10.1088/0264-9381/9/9/015)
- Dawson, K. S., et al. 2013, *Astron. J.*, 145, 10, doi: [10.1088/0004-6256/145/1/10](https://doi.org/10.1088/0004-6256/145/1/10)
- Frolov, A. V., & Frolov, V. P. 2014, *Phys. Rev. D*, 90, 124010, doi: [10.1103/PhysRevD.90.124010](https://doi.org/10.1103/PhysRevD.90.124010)
- Frolov, V. P., & Zelnikov, A. 2011, *Introduction to black hole physics* (Oxford: Oxford Univ. Press), doi: [10.1093/acprof:oso/9780199692293.001.0001](https://doi.org/10.1093/acprof:oso/9780199692293.001.0001)
- Gao, Y.-X., & Xie, Y. 2021, *Phys. Rev. D*, 103, 043008, doi: [10.1103/PhysRevD.103.043008](https://doi.org/10.1103/PhysRevD.103.043008)
- Ghosh, S. G., Amir, M., & Maharaj, S. D. 2020, *Nucl. Phys. B*, 957, 115088, doi: [10.1016/j.nuclphysb.2020.115088](https://doi.org/10.1016/j.nuclphysb.2020.115088)
- Gibbons, G. W. 1975, *Commun. Math. Phys.*, 44, 245, doi: [10.1007/BF01609829](https://doi.org/10.1007/BF01609829)
- Goroff, M. H., & Sagnotti, A. 1986, *Nucl. Phys. B*, 266, 709, doi: [10.1016/0550-3213\(86\)90193-8](https://doi.org/10.1016/0550-3213(86)90193-8)
- Hawking, S. W. 1972, *Commun. Math. Phys.*, 25, 152, doi: [10.1007/BF01877517](https://doi.org/10.1007/BF01877517)
- Herdeiro, C., Radu, E., & Rúnarsson, H. 2016, *Class. Quant. Grav.*, 33, 154001, doi: [10.1088/0264-9381/33/15/154001](https://doi.org/10.1088/0264-9381/33/15/154001)
- Herdeiro, C. A. R., & Radu, E. 2014, *Phys. Rev. Lett.*, 112, 221101, doi: [10.1103/PhysRevLett.112.221101](https://doi.org/10.1103/PhysRevLett.112.221101)
- . 2015, *Int. J. Mod. Phys. D*, 24, 1542014, doi: [10.1142/S0218271815420146](https://doi.org/10.1142/S0218271815420146)
- Hioki, K., & Maeda, K.-i. 2009, *Phys. Rev. D*, 80, 024042, doi: [10.1103/PhysRevD.80.024042](https://doi.org/10.1103/PhysRevD.80.024042)
- Horava, P. 2009, *Phys. Rev. D*, 79, 084008, doi: [10.1103/PhysRevD.79.084008](https://doi.org/10.1103/PhysRevD.79.084008)

- Horbatsch, M., Silva, H. O., Gerosa, D., et al. 2015, *Class. Quant. Grav.*, 32, 204001, doi: [10.1088/0264-9381/32/20/204001](https://doi.org/10.1088/0264-9381/32/20/204001)
- Horndeski, G. W. 1974, *Int. J. Theor. Phys.*, 10, 363, doi: [10.1007/BF01807638](https://doi.org/10.1007/BF01807638)
- Israel, W. 1967, *Phys. Rev.*, 164, 1776, doi: [10.1103/PhysRev.164.1776](https://doi.org/10.1103/PhysRev.164.1776)
- Johannsen, T. 2013, *Astrophys. J.*, 777, 170, doi: [10.1088/0004-637X/777/2/170](https://doi.org/10.1088/0004-637X/777/2/170)
- Johnson, M. D., et al. 2020, *Sci. Adv.*, 6, eaaz1310, doi: [10.1126/sciadv.aaz1310](https://doi.org/10.1126/sciadv.aaz1310)
- Kerr, R. P. 1963, *Phys. Rev. Lett.*, 11, 237, doi: [10.1103/PhysRevLett.11.237](https://doi.org/10.1103/PhysRevLett.11.237)
- Kumar, R., & Ghosh, S. G. 2020a, *Astrophys. J.*, 892, 78, doi: [10.3847/1538-4357/ab77b0](https://doi.org/10.3847/1538-4357/ab77b0)
- . 2020b, *JCAP*, 07, 053, doi: [10.1088/1475-7516/2020/07/053](https://doi.org/10.1088/1475-7516/2020/07/053)
- Mizuno, Y., Younsi, Z., Fromm, C. M., et al. 2018, *Nature Astron.*, 2, 585, doi: [10.1038/s41550-018-0449-5](https://doi.org/10.1038/s41550-018-0449-5)
- Mukherjee, S., & Chakraborty, S. 2018, *Phys. Rev. D*, 97, 124007, doi: [10.1103/PhysRevD.97.124007](https://doi.org/10.1103/PhysRevD.97.124007)
- Nicolis, A., Rattazzi, R., & Trincherini, E. 2009, *Phys. Rev. D*, 79, 064036, doi: [10.1103/PhysRevD.79.064036](https://doi.org/10.1103/PhysRevD.79.064036)
- Padilla, A., & Sivanesan, V. 2013, *JHEP*, 04, 032, doi: [10.1007/JHEP04\(2013\)032](https://doi.org/10.1007/JHEP04(2013)032)
- Psaltis, D. 2008, *Living Rev. Rel.*, 11, 9, doi: [10.12942/lrr-2008-9](https://doi.org/10.12942/lrr-2008-9)
- Psaltis, D., Perrodin, D., Dienes, K. R., & Mocioiu, I. 2008, *Phys. Rev. Lett.*, 100, 091101, doi: [10.1103/PhysRevLett.100.091101](https://doi.org/10.1103/PhysRevLett.100.091101)
- Pugliese, D., & Quevedo, H. 2018, *Eur. Phys. J. C*, 78, 69, doi: [10.1140/epjc/s10052-018-5569-7](https://doi.org/10.1140/epjc/s10052-018-5569-7)
- Raymond, A. W., Palumbo, D., Paine, S. N., et al. 2021, *The Astrophysical Journal Supplement Series*, 253, 5, doi: [10.3847/1538-3881/abc3c3](https://doi.org/10.3847/1538-3881/abc3c3)
- Roelofs, F., Fromm, C. M., Mizuno, Y., et al. 2021, *Astron. Astrophys.*, 650, A56, doi: [10.1051/0004-6361/202039745](https://doi.org/10.1051/0004-6361/202039745)
- Sako, M., et al. 2018, *Publ. Astron. Soc. Pac.*, 130, 064002, doi: [10.1088/1538-3873/aab4e0](https://doi.org/10.1088/1538-3873/aab4e0)
- Sievers, J. L., et al. 2013, *JCAP*, 10, 060, doi: [10.1088/1475-7516/2013/10/060](https://doi.org/10.1088/1475-7516/2013/10/060)
- Stelle, K. S. 1977, *Phys. Rev. D*, 16, 953, doi: [10.1103/PhysRevD.16.953](https://doi.org/10.1103/PhysRevD.16.953)
- Synge, J. L. 1966, *Mon. Not. Roy. Astron. Soc.*, 131, 463, doi: [10.1093/mnras/131.3.463](https://doi.org/10.1093/mnras/131.3.463)
- Teo, E. 2021, *Gen. Rel. Grav.*, 53, 10, doi: [10.1007/s10714-020-02782-z](https://doi.org/10.1007/s10714-020-02782-z)
- Tsukamoto, N., Li, Z., & Bambi, C. 2014, *JCAP*, 06, 043, doi: [10.1088/1475-7516/2014/06/043](https://doi.org/10.1088/1475-7516/2014/06/043)
- Tsupko, O. Y. 2017, *Phys. Rev. D*, 95, 104058, doi: [10.1103/PhysRevD.95.104058](https://doi.org/10.1103/PhysRevD.95.104058)
- Walia, R. K., Maharaj, S. D., & Ghosh, S. G. 2021. <https://arxiv.org/abs/2109.08055>
- Wei, S.-W., & Liu, Y.-X. 2013, *JCAP*, 11, 063, doi: [10.1088/1475-7516/2013/11/063](https://doi.org/10.1088/1475-7516/2013/11/063)
- Weinberg, S. 1989, *Rev. Mod. Phys.*, 61, 1, doi: [10.1103/RevModPhys.61.1](https://doi.org/10.1103/RevModPhys.61.1)
- Zajaček, M., Tursunov, A., Eckart, A., & Britzen, S. 2018, *Mon. Not. Roy. Astron. Soc.*, 480, 4408, doi: [10.1093/mnras/sty2182](https://doi.org/10.1093/mnras/sty2182)
- Zwicky, F. 1933, *Helv. Phys. Acta*, 6, 110, doi: [10.1007/s10714-008-0707-4](https://doi.org/10.1007/s10714-008-0707-4)